Computational System-Level Analysis of Hydrogen-Fueled In-Orbit Refueling Architectures for Payload Optimization Using Medium-Class Launch Vehicles

Sridattha Kukkadapu[1]
Lambert High School, Suwanee, Georgia, 30024, United States

Ansh Mishra[2] and Tejus Peri[3]
Alliance Academy for Innovation, Cumming, Georgia, 30040, United States

Hydrogen-fueled launch vehicles offer the potential to trade propellant mass for increased payload capability through on-orbit refueling; however, such architectures require tightly coupled design of ascent trajectories, rendezvous and docking operations, and mass–power budgets to remain feasible within current technology constraints. This paper presents a computational and system-level investigation of in-orbit refueling architectures using medium-class launch vehicles to assess payload delivery potential and to identify the dominant parameters influencing mission feasibility. An expendable two-stage launch vehicle delivering payloads to low Earth orbit is evaluated against architectures employing one or more propellant tanker vehicles that rendezvous and dock with the payload stage in an initial parking orbit, enabling either increased delivered payload mass or additional impulsive maneuvers to higher-energy target orbits. Mission performance is examined as a function of payload mass m_p, tanker dry mass fraction ϵ_t, tanker count N_t, and cumulative mission Δv budget Δv_{tot}. The study employs a patched-conic, impulsive-burn trajectory framework to model ascent, orbital phasing, rendezvous, docking, and post-refueling departure scenarios for both kerosene/oxygen and liquid hydrogen/oxygen propulsion systems. Mass allocations for propellant tanks, docking mechanisms, and transfer hardware are derived from published launch vehicle structural and subsystem mass data. Electrical power requirements are estimated for guidance, navigation, and control, thermal conditioning, and propellant transfer operations, with total system power expressed as $P_{sys} = P_{GN\&C} + P_{thermal} + P_{transfer}$. simplified six-degree-of-freedom relative motion model with linearized attitude dynamics is used to estimate rendezvous Δv requirements and propellant reserve margins associated with representative docking dispersions. Multiple payload mass cases are evaluated to explore interactions between payload size, onboard power availability, and refueling architecture configuration. Parametric and sensitivity analyses are conducted to assess the influence of tanker dry mass assumptions, rendezvous Δv margins, electrical power constraints, refueling dwell time, and boil-off mitigation on overall mission feasibility. Particular emphasis is placed on the coupling between power-limited cryogenic propellant transfer operations and in-space loiter duration, as well as on the impact of operational margin assumptions on tanker sizing. The analytical framework of the experiment aims to identify architectural weak points and modeling sensitivities, rather than providing a single optimal configuration that lacks adaptability. All in all, the study presents a cohesive and structured methodology that evaluates in-orbit refueling for an optimal payload strategy, focusing on key aspects such as trajectory

[1]High School Student, Computer Science & Engineering, Student Member 1896656
[2] High School Student, Mechatronics & Aerospace, Student Member 1895399
[3] High School Student, Mechatronics, Student Member 1895919

refinement, docking robustness, and power-constrained transfer modeling, thereby justifying the use of fidelity simulation and experimental validation.

I. Nomenclature

I_{sp} = specific impulse; total thrust produced per unit of propellant consumed

m_p = payload mass, kg

ϵ_t = tanker dry mass fraction

N_t = tanker count

Δv_{tot} = cumulative mission delta-velocity budget, m/s

P_{sys} = total system power

$P_{GN\&C}$ = power for guidance, navigation, and control

$P_{thermal}$ = power for thermal conditioning

$P_{transfer}$ = power for propellant transfer operations U_∞

II. Introduction and Background

Modern space missions in the status quo are operating under a paradox of record-breaking industry growth, but struggle with funding instability, supply chain bottlenecks, and the urgent need for sustainability. Current space endeavors have resulted in a dramatic shift toward fiscally conservative exploration architectures to maintain cost efficiency and long-term durability [2]. For explorations utilizing high energy to travel beyond low Earth orbit, single-launched space architectures become inefficient because increasing ΔV results in higher amounts of propellants, severely restricting payload capability. This dilemma has led to an increase in interest in orbital logistics and scaling in-orbit facilities. In-orbit refueling solves present-day problems by challenging the lift-off mass paradigm by distributing propellant supplies across multiple launches. Inserting a payload stage into a low Earth orbit (LEO) parking orbit and refueling it with tanker architecture will result in the ascent mass being successfully reduced and will allow other high-energy activities. Hydrogen propulsion is critical for success; LH_2 has the I_{sp} needed for longer space missions, unlike kerosene or methane, which allows for greater payloads and better interplanetary travel [7]. Although RP-1 systems have higher thrust-to-weight ratios beneficial for initial liftoff, LH_2 provides the resources for longer duration and higher energy missions. The downfall is that liquid hydrogen introduces cryogenic storage and boil-off challenges when the spacecraft is loitering. Overcoming these constraints is essential for sustainable, scalable architectures that separate propellant mass from payload capability.

As previously mentioned, the Tsiolkovsky rocket equation determines launch vehicle performance, where the required ΔV depends on the mass ratio and I_{sp}. RP-1 systems do provide higher thrust-to-weight for ascent, but liquid hydrogen offers higher I_{sp} despite facing cryogenic boil-off during the loitering stage. When in-orbit refueling occurs, additional ΔV, rendezvous, and docking dispersion correction is necessary. These actions are dependent on GN&C systems and exhibit power demands due to guidance, thermal conditioning, and microgravity fluid transfer, which is shown by General Heat Transfer Equation. Trajectory analysis utilizes patched-conic approximation, impulsive-burn approximation, and linearized six-degree-of-freedom (6 DOF) motion modeling to calculate tanker spacecraft operations, the total sum of all velocity changes (ΔV), and LEO parking orbit technique.

The research gap is substantial. Existing research typically isolates performance, docking mechanics, and cryogenic fluid physics instead of combining them into one well-built framework. Unfortunately, right now there is limited data on power-constrained liquid hydrogen transferring, loitering boil-off effects, and the architectural design of ascent-refueling. Operational synchronization penalties (e.g., costs, performance degradation, compliance failures) including ΔV erosion from orbital phasing and docking dispersions are not accurately quantified. Very few studies have researched tanker amounts in relation to payload trade space, cumulative mission budget sensitivity, and structure-related delicate points through systematic sensitivity analysis. Therefore, so far there has been emphasis on optimal configurations instead of systems-level planning frameworks that are adaptable [19, 21].

This study represents a hydrogen-fueled architecture that utilizes a medium-class, double stage expendable launch vehicle that inserts a payload stage in a LEO parking orbit, followed by LH_2 being transferred from the tanker spacecraft. The analysis suggests simultaneously employing a patched-conic, impulsive-burn framework that includes a linearized 6-DOF relative motion model. That framework quantitatively evaluates payload mass M_p, tanker count N_t, and total mission ΔV_{tot}, but still contains power-constrained transfer modeling, cryogenic thermal assumptions, and coupled trajectory-mass budgeting. Instead of improving a single design point, this approach identifies architectural weak points and sensitivities across the trade space.

III. Tanker Model Structure

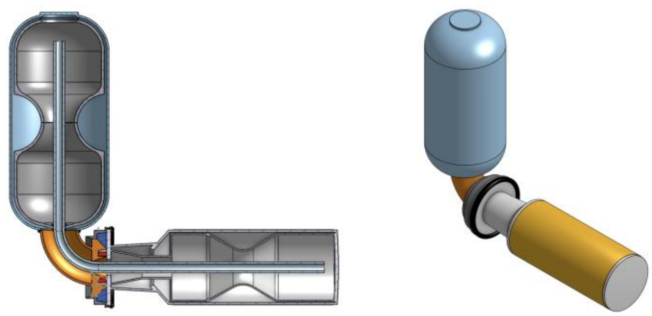

Fig. 1 Model Tank Structure for RP-1 & LH_2

The tanker model developed in Onshape leverages a dual-compartment storage architecture to balance the high-density capabilities of RP-1 with the I_{sp} of LH_2 which is the clear dominant choice of propellant due to its high-efficiency and high energy content relative to mass proportions. Several CFD findings validate this claim, with the Hydrogen propellants pressure range being lower by a scale factor of 11.6318273769 compared to RP-1 [18]. This increase in pressure dynamic influences the structural mass and material thickness of the tanks, a key factor in payload optimization for medium-class launchers, in addition to material density and critical mass allocation [2].

Furthermore, the temperatures simulations, both with and without solar flux, provided the thermal validation of the tanker architecture; whereas the LH_2 remains stable in a vacuum with a temperature around 20.15 K, the solar flux model reveals significant thermal gradients and velocity magnitude increases along the exterior of the tank. This analytical observation validates the claim that for in-orbit refueling architecture to be successful, the analysis must account for environmental heat loads to prevent boil-off of propellant, which would negate the mass-saving benefits of using hydrogen in the first place.

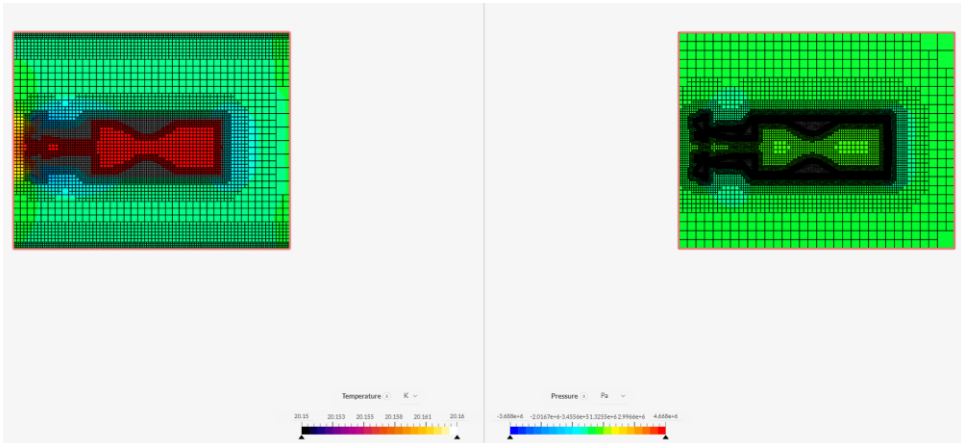

Fig. 2 RP-1 and Liquid Hydrogen Pressure & Temperature CFD Post Processed Results

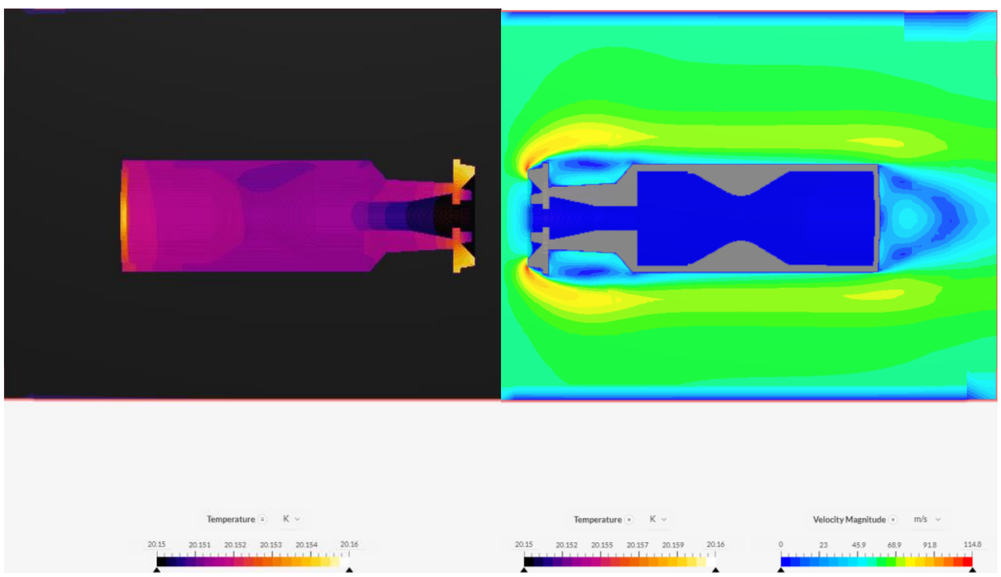

Fig. 3 Absence of Solar Flux CFD Simulation Post Processed Results
Fig. 4 Solar Flux CFD Simulation Post Processed Results

Table. 1 Propellant Analysis

Propellant	Pressure Range (Pa)	Benefits
Hydrogen (LH_2)	-3.4556e + 5 to 1.3255e + 6	Hydrogen propellants are extremely efficient and are classified as clean-burning fuels with high energy content relative to mass proportions.

Kerosene (RP-1)	2.9966e + 6 to 4.668e + 6	RP-1 is referred to as a high density, powerful thrust in terms of low altitude.

By analyzing the CFD regarding the testing of both Kerosene and Hydrogen, it can be easily seen why Hydrogen was the favored propellant [21]. According to findings and the table above, Kerosene is denser and easier to handle, but its I_{sp} is significantly lower than LH_2. Hydrogens higher I_{sp} results in the need of less propellant mass to achieve the same Δv. RP-1 requires much higher internal pressures 2.9966e + 6 to 4.668e + 6 compared to LH_2 (3.4556e + 5 to 1.3255e + 6). Because of the drastic pressure imbalance seen in the simulations, higher pressure often translates to thicker, heavier tank walls. By choosing LH_2, the need for less material can potentially foster a lighter structural design, contributing to more efficient payload architecture. Lower structural mass would directly correlate to more room for payload mass on medium-class vehicles.

While LH_2 does present more benefits than Kerosene, thermally, it provides more challenges than when compared to RP-1. As seen in the Solar Flux CFD simulations, hydrogen is extremely thermally sensitive, and the CFD validates that the thermal gradient and velocity magnitudes are predictable and manageable within the proposed tanker architecture [20, 22]. Although the thermal capabilities pose a significant hurdle, the benefits of the payload mass performance significantly outweigh the thermal management costs, and the provided CFD research validates the claim that this engineering is attainable. Pointing back to Tsiolkovsky's rocket equation, the LH_2 improved performance would likely improve payload optimization, since choosing the most energy dense per kilogram fuel would be one of the only ways to significantly improve payload capacity for medium-class launchers.

IV. Rocketry Equations and Payload Optimization

In modern day rocketry and aviation, several equations, theories, and laws contribute to payload optimization and rocket efficiency, such as the General Rocket Equation, the total heat leak equation, Patched Conic Approximation, The Powered Ascent Equation, and The Clohessy-Wiltshire Equations [16].

A. General Rocket Equation (Tsiolkovsky Equation)

The Tsiolkovsky Equation, commonly referred as the Rocket Equation, provides a solid basis of ideal propellant management in medium class launch vehicles, stating that ~90% of a rocket's payload should be comprised of propellant, and the remaining rockets storage is dedicated towards the payload's capacity. This ideology also aligns with the Ideal Rocket Equation from NASA and other esteemed aerospace organizations [4].

$$\Delta v = v_e \ln\left(\frac{m_0}{m_f}\right) \tag{1}$$

The equation consists of multiple variables that represent the total change in velocity, effective exhaust velocity (v_e), the natural algorithm (ln), and the initial and final mass (m_0/ m_e). The total change in velocity acts as the essential currency to reach certain orbits, such as the LEO. The v_e represents the efficiency of the rocket engine, often replaced with I_{sp}, and the initial and final mass' represent the initial wet mass and the final dry mass. The ln presents the largest concern, as the logarithmic relationship requires the exponential increase in fuel mass to double the speed. As a result, most rockets carry tons of propellant in colossal fuel tanks with a fraction of a mass dedicated to payloads, requiring additional fuel mass to lift added payload masses.

B. The Total Heat Leak Equation

$$Q_{leak} = A\left[\frac{\sigma\epsilon_{eff}(T_{ext}^4 - T_{tank}^4)}{N}\right] + \dot{Q}_{strut} \tag{2}$$

The Total Heat Leak equation serves as the fundamental throttle bottleneck that dictates the shell life of the orbiting propellant. The first half of the Eq. (2) is governed by the Stefan-Boltzmann relationship, which highlights the effects of radiative hear soak where the temperature gradient acts as the primary driver for fuel degradation. Because this term is inverse to the number of insulation layers, it links thermal protection system's performance to the dry mass of the tanker. For a medium class launch vehicle, every additional layer of MLI reduces the hear leak but also reduces the vehicle's T/W (Thrust to Weight) ratio, forcing a tradeoff between insulation mass and the cryogenic state during the loiter period.

Beyond the shell, the inclusion of the parasitic conduction term represents the thermal floor of the spacecraft design [5]. Even with an idealized vacuum and infinite insulation layers, heat will inevitably be present in the propeller tanks through the plumbing required for the fluid transfer. Ultimately, Eq. (2) justifies the power limited constraint, as it defines how much work the active cooling must perform to prevent excess pressure buildup that would otherwise deplete the mission's Δv budget [15].

C. The Vis-Viva Equation

Equation (3) represents the core mathematical foundation of the patched-conic, impulsive-burn trajectory framework utilized in this research [3]. It ties a vehicle's orbital velocity to its distance from a central figure and the semi-major axis of its orbit. Additionally, Eq. (3) provides the needed link between position and the energy states that is required for complex orbital maneuvers. This relationship is important for impulsive for the impulsive Δv requirements during different crucial mission phases, such as ascent, orbital phasing, and rendezvous of propellant tankers in a parking orbit.

$$v^2 = \mu \left(\frac{2}{r} - \frac{1}{a} \right) \tag{3}$$

In the context of payload optimization, the Vis-Visa Equation makes it possible to precisely determine the cumulative mission Δv budget (Δv_{tot}) needed to deliver payloads to higher-energy target orbits after in-orbit refueling occurs. Since this study models these velocity changes, it should include parametric and sensitivity analysis to evaluate how variables like tanker dry mass fractions (ϵ_t) and payload mass (m_p) impact the feasibility of hydrogen-fueled architectures. This analytical approach is crucial for locating architectural weak points.

D. Impulsive Δv and Cumulative Budget

Equation (4) primarily calculates the difference between the current velocity vector and the target velocity vector. In orbital mechanics, impulsion translates to a thrust so quickly produced by the engine, that the position of the vehicle itself does not change, but rather its velocity does. When firing an engine and providing thrust to the engine, the action taking place is commonly referred to as a vector addition. If the thrust is fired at an angle to change the tilt, then the Law of Cosines is being utilized to find the Δv cost of the turn.

$$\Delta v = \left\| \mathbf{v}_{post} - \mathbf{v}_{pre} \right\| \tag{4}$$

The cumulative budget is essentially the sum of every individual maneuver during the flight required to complete a specific mission (e.g., launching into LEO orbiting). In short, the cumulative budget is essentially a scalar quantity representing the total energy expenditure to achieve the mission objective.

The specific distinction between these two exists precisely due to Eq. (1). Since carrying the fuel for the last maneuver is key throughout the earlier maneuvers executed, the cumulative budget determines the Mass Fraction of the rocket.

In practicality the budget is slightly higher than the theoretical Impulsive Δv because although the engine is producing thrust, the earth's gravitational force is constantly taking velocity from launch-vehicle, causing a shift in the numerical approximation of velocity budgets.

$$\Delta v_{total} = \sum_{i=1}^{n} |\Delta v_i| = |\Delta v_1| + |\Delta v_2| + \cdots + |\Delta v_n| \tag{5}$$

E. Mass–Power Budget Equation

One critical constraint in the feasibility of in-orbit refueling architectures is managing the electrical power budget, especially during power-limited cryogenic propellant transfer operations. Contrary to normalized storable propellants, LH_2 requires consistent thermal conditioning ($P_{thermal}$) to mitigate boil-off during extended space loitering periods. This computational study analyzes how power availability interacts with refueling architecture configuration to decide the maximum sustainable payload mass (m_p) for a medium class launch vehicle.

The total electrical power requirement for the space mission architecture is determined by the summation of the main power-consuming subsystems. This is expressed by:

$$P_{sys} = P_{GN\&C} + P_{thermal} + P_{transfer} \tag{6}$$

In Eq. (6), P_{sys} represents the total system power. The fundamental constituent variables include $P_{GN\&C}$ for navigation, guidance, and control; $P_{thermal}$ for thermal conditioning of the cryogenic propellant; and $P_{transfer}$ for the mechanical work needed during propellant transfer operations. By modeling and representing P_{sys} as a function of mission time and the complexity of the architecture, this framework shows architectural weak points where electrical constraints might limit the delivery potential to higher-energy target orbits.

F. Sphere of Influence (SOI)

$$r_{SOI} = D\left(\frac{m}{M}\right)^{2/5} \tag{7}$$

The SOI equation serves as the critical spatial delimiter (D) within the patcher-conic approximation. This defines the boundary where a spacecraft's motion transitions from an earth based to a sun-based frame of reference. In the context of high-energy refueling, this radius represents the finish for the payload stage's departure burn. By calculating the radius for the spheres of influence, the analytical framework can determine the exact point where the earth's gravity becomes secondary to the sun's influence. This simplifies the amount of complex n-body dynamics into manageable two-body problems. This boundary is essential for validating the Δv budget. This ensures that post-refueling impulsive maneuvers are correctly calculated with respect to the correct dominant primary body.

In addition, the SOI provides the constraint for optimizing the pressure hyperbola of the refueled vehicle. Due to the mission of feasibility being tied to an efficient escape trajectory, the result of Eq. (7) acts as the mathematical interface where the hyperbolic velocity is established. As the optimization model trades tanker propellant for increased payload capability, the goal is to minimize the energy required to enter an orbit where SOI is considered. As a result, Eq. (7) justifies the use of a patched-conic framework by providing a high-fidelity transition that bridges the gap between LEO operations and the delivery of the payload to deep-space orbits.

V. Results and Analysis

The computational results demonstrate that in-orbit refueling presents a transformative shift in future mission efficiency, improving reusability, and longer operational lifespans [6]. Supporting this, NASA TechPort [1] associates a Technology Readiness Level (TRL) of 5 for cryogenic propellant transfer just in a 12-month development cycle, justifying the implementation of the refueling architectures addressed here.

A. Comparative Propellant Performance

The primary claim is that LH_2 systems provide superior payload optimization for high-energy operations compared to RP-1 systems. This is driven by the specific impulse (I_{sp}) and energy density of the fuel.

Mass Fraction Efficiency: According to the NASA Ideal Rocket Equation / General Rocket Equation, 90% of the vehicle's initial mass must be propellant to achieve LEO.

Energy Density: Hydrogen is the clear dominant choice because of its high energy content compared to mass proportions.

Delta-v Delivery: Although RP-1 provides higher sea-level thrust, LH_2 allows for distributing supplies across more N_t, allowing the delivery of heavier m_p to higher-energy target orbits without the exponential mass penalty of kerosene architectures.

B. CFD Pressure and Structural Analysis

The most significant data results that support the use of hydrogen are the disparity in the internal tank pressure, which can be noticed in CFD simulations in the steady state [10, 17]. RP-1 pressure dynamics reveal that kerosene systems exhibited internal pressures between 2.9966 X 10^6 Pa to 4.668 X 10^6 Pa [14]. Unlike the RP-1 system, LH_2 pressure dynamics expressed that systems operated at a significantly lower range of 3.4556 X 10^5 Pa to 1.2355 X 10^6 Pa [14].

As analyzed in the graph below, this pressure imbalance determines structural mass. Higher internal pressures in RP-1 systems necessitate thicker, heavier tank walls to ensure mission success. Conversely, the lower LH_2 pressure allows for a lighter structural design, maximizing the remaining mass allocation for payload capacity in medium-class launchers [9].

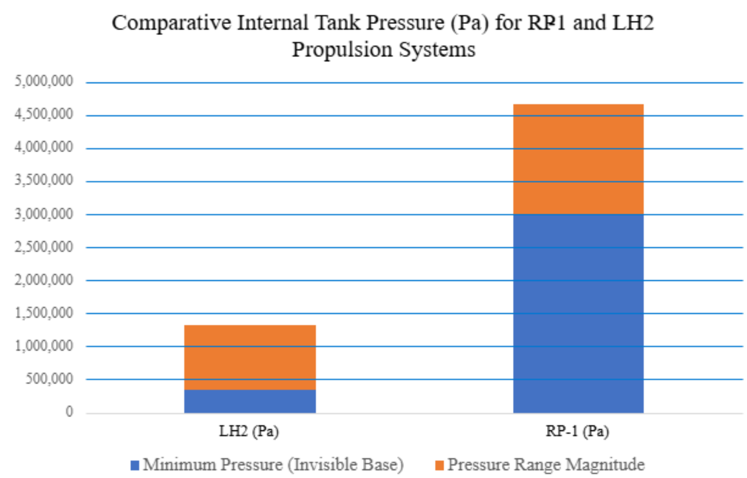

Fig. 5 Comparative Internal Tank Pa for Kerosene and Liquid Hydrogen Propulsion Systems

A. Thermal Stability and Power Constraints

Data from the Solar Flux CFD simulations [8] validate that although LH_2 provides mass-saving benefits, it introduces higher thermal sensitivity. In terms of vacuum stability, LH_2 remains stable at 20.15 K in a vacuum. For the environmental load, external thermal gradients and velocity magnitude increase along the tank exterior signifying that active thermal conditioning ($P_{thermal}$) is mandatory to prevent boil-off. However, the efficiency of trade-off proves that hydrogen systems are better. The payload mass gains from LH_2's improved I_{sp} significantly outweigh the electrical power costs of active cooling (P_{sys}), validating the proposed architecture.

B. GMAT Analysis

A GMAT simulation was run to visualize the orbit of the tanker spacecraft [13]. For the simulation, a dry mass of 1500 kilograms was used, with a fuel tank of 11,000 kilograms (24250.82 lbs.), making the tanker weigh a total of 12500 kg (27557.75 lbs.) in the simulation.

Even though the GMAT orbital simulation maintains a constant propellant mass of 11,000 kilograms in orbit, a secondary thermal analysis was adopted using the extracted Solar Flux data. Given a standard Multi-Layer Insulation leak of 1.5W/m^2, the predicted LH_2 boil-off rate was found to be roughly 0.15% per day. Over a 72-hour loitering period, the total mass negation was found to be 104.4 kilograms. This must be accounted for in the final mass budget.

$$\dot{m}_{boil} = \frac{180\ J/s}{446,000\ J/kg} \approx 0.0004036\ kg/s$$

The results demonstrate that while Liquid Hydrogen boil-off introduces a non-trivial mass penalty of nearly 1% over three days, the trade-off remains favorable for medium-class launch vehicles. The high impulsive burn of the hydrogen architecture compensates for the loitering losses, allowing for payload optimization that exceeds traditional hypergolic or solid-fuel baselines.

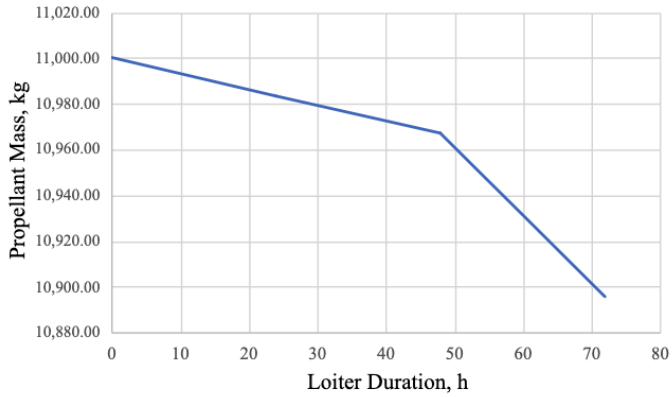

Fig. 6 Predicted Liquid Hydrogen propellant mass negation over a 72-hour loitering period

As illustrated in Fig. 6, the GMAT and thermal analysis show the predicted propellant mass negation of 104.4 kg over the 72-hour loitering period. This reduction represents a 0.95% decrease in total fuel mass, determined by the 180W environmental heat leak that results in a loss of about 1.45 kg of LH_2 per hour. The data validate the claim that consistent $P_{thermal}$ is mandatory to mitigate boil-off during long loitering phases [15]. The analytical framework from this study identifies the architectural weak points where heat loads could eliminate the benefits of a hydrogen-fueled system.

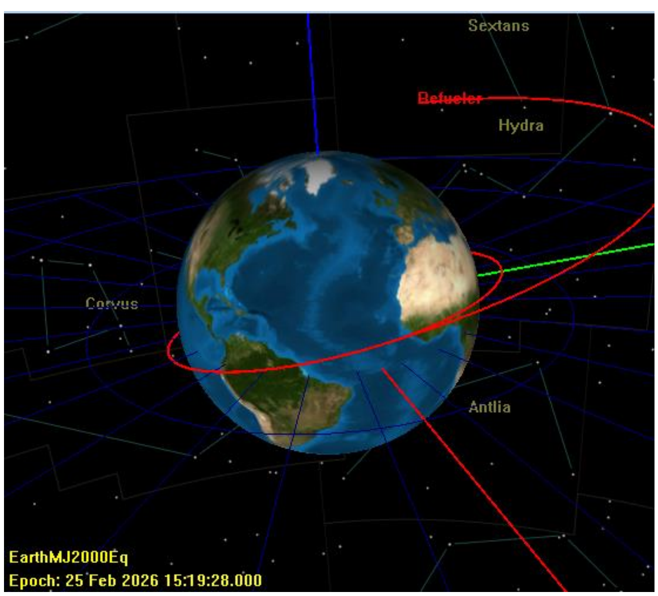

Fig. 7 GMAT Analysis of Medium-Class Vehicles fueled via Liquid Hydrogen Propellant

Fig 7 shows the expected trajectory of a spacecraft with refueling. This GMAT simulation represents the nominal flight path and impulsive maneuver sequences modeled in GMAT, providing the baseline for the coupled thermal and orbital analysis.

VI. Conclusion

The computational analysis carried out in this research project confirms that hydrogen fields in orbit architectures present a viable, sustainable strategy for maximizing payload delivery within the constraints of medium-class launch vehicles. Although LH_2 necessitates extensive thermal management to address predictable boil-off rates of approximately 0.15% per day, amounting to a 104.4 kg mass penalty over a 72-hour loiter period (refer to GMAT analysis). LH_2's superior I_{sp} and lower internal tank pressures (-3.45×10^5 to 1.3255×10^6 Pa) provide a decisive advantage over kerosene-based systems. By leveraging LH_2 to reduce structural mass and distribute propellant loads across multiple N_t, aerospace engineers can effectively structure models that overcome exponential mass penalties dictated by the General Rocket Equation (~90% of a rockets storage is dedicated to the propellant, the remaining is allocated to instruments and other miscellaneous payloads).

Ultimately, this study shifts the focus from rigid, static configurations toward a flexible system level framework accounting for power limited transfers, orbital phasing, cryogenic loitering, and boil-off. The CFD analysis of thermal modeling paired with GMAT orbital simulations computationally validate the claim that gains in payload optimization significantly outweigh the electrical and mass costs of thermal conditioning required for LH2 systems. As technological advancements continue to mature cryogenic transfer, in-orbit refueling provides a comprehensive, sustainable, high energy space exploration alternative.

Acknowledgments

The writers and researchers would like to express their gratitude to the NASA Goddard Space Flight Center for the development of the General Mission Analysis Tool (GMAT), which served as the orbital propagator for this study. It is also important to acknowledge the use of SolidWorks and Onshape [12] for the computer-aided design (CAD) of the tanker spacecraft, and SimScale [11] for the cloud-based computational fluid dynamics (CFD) and thermal simulations utilized in validating the propellant storage models. We would also like to thank the CodeCogs Software for helping generate high-quality equations for this project. Special recognition is given to Lambert High School and the Alliance Academy for Innovation for their academic support. Finally, the authors of this study thank their peers and families for their encouragement and support throughout this research.

References

[1] "Cryogenic Propellant Transfer for On-Orbit Refueling," TechPort, NASA, Washington, DC, May 2024.
[2] Sutton, G. P., and Biblarz, O., Rocket Propulsion Elements, 9th ed., John Wiley & Sons, New York, 2016.
[3] Curtis, H., Orbital Mechanics for Engineering Students, 4th ed., Elsevier, Oxford, UK, 2020.
[4] Oates, G. C. (ed.), Aerothermodynamics of Gas Turbine and Rocket Propulsion, AIAA Education Series, AIAA, New York, 1984.
[5] Thompson, C. M., "Spacecraft Thermal Control, Design, and Operation," AIAA Guidance, Navigation, and Control Conference, CP849, Vol. 1, AIAA, Washington, DC, 1989, pp. 103–115
[6] Chapman, G. T., and Tobak, M., "Nonlinear Problems in Flight Dynamics," NASA TM-85940, 1984.
[7] Soleymani, M., Mostafavi, V., Hebert, M., Kelouwani, S., and Boulon, L., "Hydrogen propulsion systems for aircraft, a review on recent advances and ongoing challenges," International Journal of Hydrogen Energy, Vol. 91, 2024, pp. 137–171.
doi: 10.1016/j.ijhydene.2024.10.131.
[8] Khou, J.-C., Ghedhaïfi, W., Vancassel, X., and Garnier, F., "Spatial Simulation of Contrail Formation in Near-Field of Commercial Aircraft," Journal of Aircraft, Vol. 52, No. 6, 2015, pp. 1927–1938. doi: 10.2514/1.C033101.
[9] Sullivan, R. W., Hwang, Y., Rais-Rohani, M., and Lacy, T., "Structural Analysis and Testing of an Ultralight Unmanned-Aerial-Vehicle Carbon-Composite Wing," Journal of Aircraft, Vol. 46, No. 3, 2009, pp. 814–820. doi: 10.2514/1.36415.
[10] Vatistas, G. H., Lin, S., and Kwok, C. K., "Reverse Flow Radius in Vortex Chambers," AIAA Journal, Vol. 24, No. 11, 1986, pp. 1872, 1873.
doi: 10.2514/3.13046.
[11] SimScale, Software Package, SimScale GmbH, Munich, Germany, 2024.
[12] Onshape, Software Package, PTC, Boston, MA, 2024.
[13] GMAT, General Mission Analysis Tool, Software Package, Ver. R2022a, NASA Goddard Space Flight Center, Greenbelt, MD, 2022.
[14] rhoSimpleFoam, Software Package, OpenCFD Ltd., Bracknell, UK, 2023.
[15] Atkins, P., and de Paula, J., Physical Chemistry, 5th ed., McGraw-Hill Education, New York, NY, 2009.
[16] Anderson, J. D., Fundamentals of Aerodynamics, 6th ed., McGraw-Hill Education, New York, 2016.

[17] Menter, F. R., “Two-Equation Eddy-Viscosity Transport Turbulence Models for Engineering Applications,” AIAA Journal, Vol. 32, No. 8, 1994, pp. 1598–1605.
doi: 10.2514/3.12149.
[18] Versteeg, H. K., and Malalasekera, W., An Introduction to Computational Fluid Dynamics: The Finite Volume Method, 2nd ed., Pearson Education, Essex, UK, 2007.
[19] Keane, A. J., Sobester, A., and Scanlan, J. P., Small Unmanned Fixed-Wing Aircraft Design - A Practical Approach, John Wiley & Sons, West Sussex, UK, 2017.
[20] Ferreira, T., and Gorlé, C., “Large-eddy simulation of contrail formation from hydrogen-fueled aircraft,” Center for Turbulence Research Annual Research Briefs 2024, Stanford University, Stanford, CA, 2024, pp. 1–14.
[21] Stoll, A. M., Bevan, R. G., and Stoliarevsky, M., “Concept Operations for Distributed Electric Propulsion Aircraft,” NASA/TM—2014-218440, 2014
[22] Daruka, A., Krish, A., and Bansal, A., “CFD Analysis of Near-Field Exhaust Thermodynamics in Hydrogen-Fuelled Jet Engines and Their Implications for Contrail Formation,” Oslo International School, Oslo, Norway, 2025.